Finite-temperature magnetism of disordered Fe-Cr alloys

Y. Kakehashi
Department of Physics, Hokkaido Institute of Technology, Teine-Maeda, Nishi-ku, Sapporo 006, Japan
(Received 21 October 1986)

A theory of the local-environment effects (LEE) at finite temperatures has been extended to the antiferromagnetic case in order to investigate the magnetism of Fe-Cr alloys in the ferromagnetic and antiferromagnetic states. The magnetic phase diagram of Fe-Cr alloys, magnetization and sublattice magnetization versus concentration curves, internal-field distribution function, high-field susceptibility, paramagnetic susceptibility, and other magnetic quantities have been calculated at finite temperatures by making use of the theory of the LEE. It is found that the Fe local moments show a strong LEE in the antiferromagnetic as well as in the ferromagnetic one. The nature of the LEE in the antiferromagnetic state changes with the disappearance of the gap in the density of states. An overall agreement between various experiments and the present theory is obtained, but the extended interactions between local moments have to be taken into account to explain the low-temperature properties of Fe-Cr alloys such as the spin-glass state.

I. INTRODUCTION

Since many transition-metal alloys are near the Stoner boundary, at which the local magnetic moments collapse,[1] the magnetic states are often influenced by the magnetic and atomic configurations at neighboring sites. This is called the local-environment effect (LEE).[2–5] Such effects also appear in the strong magnetic alloys with ferromagnetic and antiferromagnetic interactions because of the change of direction of local moments (LM's) due to the configuration of surrounding of LM's and the competing interactions.[6,7] The LEE is therefore important for the magnetism of the transition-metal alloys.

The single-site approximation[8] (SSA) for alloys completely neglects the LEE. The present author therefore developed a theory for the LEE at finite temperatures.[9,10] It uses a two-field functional-integral method which describes local moments as well as itinerant features in transition metals.[11–15] The fluctuations of LM's with respect to the configurational average are taken into account by means of the distribution-function method developed by Matsubara and Katsura.[16,17] Therefore the spin-glass state, the LEE on the amplitude of LM's, and the atomic short-range order are included in the theory.

In a series of papers on alloy problems, we have investigated the finite-temperature magnetism of Fe-Ni,[10] Ni-Mn,[9,18,19] and Fe-V alloys[20] by using the theory of the LEE. We have shown for the Fe-Ni alloys that the anomalous Fe-Fe coupling in the fcc lattice (i.e., an antiferromagnetic coupling for small-amplitude Fe LM's and a ferromagnetic coupling for large amplitude) is responsible for the strong LEE in the vicinity of the ferromagnetic instability of Fe-Ni Invar. Rapid but continuous deviation from the Slater-Pauling curve, deviation from the Brillouin curves, and temperature- and concentration-dependences of the broad distribution of internal fields seen by Fe have been explained from the viewpoint of the LEE.

Ni-Mn alloys have been investigated as a typical system with competing interactions: the ferromagnetic couplings between Ni LM's and between Mn and Ni LM's, and the antiferromagnetic coupling between Mn LM's. The magnetization versus concentration curve with a peak, the large change of the paramagnetic susceptibility due to the atomic short-range order, the double-stage magnetization versus temperature curves in Ni_3Mn, and the asymmetry of the high-field susceptibility around the critical concentration have successfully been explained using LEE theory. In particular, spin-glass solutions appear in this alloy after the disappearance of ferromagnetism with increasing Mn concentration. The spin-glass temperature T_g was shown to be influenced strongly by the atomic short-range order as is the magnetization and the Curie temperature.

In the investigations of Fe-V alloys we first checked the validity of the theory by comparing our theory with cluster coherent-potential-approximation (CPA) calculations for the ground state. It has been found that the present theory is reasonable at finite concentrations. A change of the magnetism from the LM type to Pauli paramagnetism in Fe-V alloys has been investigated. The Curie temperature maximum as a function of the concentration was shown to be due to the alloying effect. The broad internal field distribution and the concentration dependence of the paramagnetic susceptibility have also been explained by the theory of LEE.

In the present paper we investigate the finite-temperature magnetism of Fe-Cr alloys by means of our theory of the LEE. Our question is to what extent one can understand the complicated magnetism of Fe-Cr alloys by means of LEE theory.

Disordered Fe-Cr alloys form a bcc structure over a full concentration range, and show ferromagnetism, a spin-glass state, and antiferromagnetism with increasing Cr concentration.[21,22] The Curie temperature T_C shows a small maximum at 5 at. % Cr,[23] which is not explained by the rigid-band theory, and goes to zero at 81 at. % Cr. Mössbauer experiments indicate the existence of various

magnetic states of LM's over a wide range of concentration (20–90 at. % Cr), showing up the importance of the LEE.[24–27]

The alloys show antiferromagnetism at more than 84 at. % Cr. The Néel temperatures T_N increase with increasing Cr concentration. The alloys cause a transition from antiferromagnetism to an incommensurate spin-density wave at a few atomic percent Fe,[28,29] which is outside the scope of our present investigations. In a small concentration regime between the ferromagnetic and antiferromagnetic states (i.e., 81–84 at. % Fe) the Fe-Cr alloys are considered to be in the spin-glass state.[21,22] The high-field susceptibility shows a broad and large maximum near there.[30]

Theoretical investigations of Fe-Cr alloys had been limited to the ground state for many years. The concentration dependence of the average LM has been explained well by Hasegawa and Kanamori[31] and Frollani *et al.*[32] on the basis of the CPA. A calculation in the antiferromagnetic state has been performed by Jo within the CPA.[33] A second-order transition from the antiferromagnetic state to a paramagnetic state was obtained.

Finite-temperature calculations in the ferromagnetic regime have recently been done by Hasegawa within the SSA.[8] He calculated the concentration dependence of T_C, the magnetization-versus-temperature curves, and the paramagnetic susceptibilities. He found that the partial susceptibilities of Cr do not follow the Curie-Weiss law. Calculated Curie temperatures decrease monotonically with increasing Cr concentration against the experimental fact. Unfortunately he did not investigate the magnetism near the ferromagnetic instability, which is both theoretically and experimentally interesting. Furthermore, the finite temperature calculation in the antiferromagnetic state has not been performed yet even within the SSA.[8] Thus the magnetic properties of Fe-Cr alloys at finite temperatures remain almost unresolved. The present work is the first systematic investigations of the magnetism of Fe-Cr alloys at finite temperatures from the theoretical viewpoint.

Hitherto the theory of the LEE has been limited to the ferromagnetic state. We extend it to the antiferromagnetic state in the following section. We adopt the degenerate-band Hubbard model instead of the single-band model according to the recent development of the two-field functional-integral method.[34] A few comments on degeneracy and quantum effects on the amplitude of the LM will be made.

In Sec. III we explain the numerical calculations and parameters. Then we discuss the magnetic phase diagram in Sec. IV. Concentration dependence of calculated LM and the internal-field distribution seen by Fe will be presented in Sec. V. Strong concentration dependence of Fe LM's in various local environments is found in the antiferromagnetic state. It is related to the disappearance of the gap in the density of states (DOS). In Sec. VI, temperature variations of calculated magnetic quantities are shown. It is found that Fe LM's in each environment show an interesting temperature dependence in the antiferromagnetic state because of the competition between the ferromagnetic and antiferromagnetic couplings. Calculated internal field distribution functions are compared with the Mössbauer experiments. The origin of a shoulder in the spectra near the critical concentration of the ferromagnetism is presented. In Sec. VII the high-field susceptibility, the effective Bohr magneton number, and the Weiss constant in the paramagnetic susceptibility χ_p are presented as a function of concentration. Origin of a broad peak of high-field susceptibility is also discussed there. We finally summarize in Sec. VIII our physical picture for the magnetism of Fe-Cr alloys, and discuss remaining problems.

II. THEORY OF THE LEE IN FERROMAGNETIC AND ANTIFERROMAGNETIC ALLOYS

We adopt the degenerate-band Hubbard model, and apply the two-field functional-integral method. The free energy F is then given as follows in the static approximation:[34]

$$F=-\beta^{-1}\ln\int\prod_i\left[\frac{\beta\tilde{J}_i}{4\pi}\right]^{1/2}d\xi_i e^{-\beta E(\xi)}\ . \tag{2.1}$$

Here β is the inverse temperature. $\tilde{J}_i$ is an exchange parameter defined by

$$\tilde{J}_i=\frac{1}{2D}U_i+\left[1+\frac{1}{2D}\right]J_i\ , \tag{2.2}$$

U_i (J_i) being a Coulomb (exchange) integral on site i. D is the degeneracy of the bands (i.e., $D=5$). Because of the strong local electron correlations even at finite temperatures, $\tilde{J}_i$ should be regarded as a reduced parameter.[35]

The energy functional $E(\xi)$ in Eq. (2.1) consists of the free energy for the one electron Hamiltonian $H(\xi)$ with exchange fields $\{\xi_i\}$, and the Gaussian term

$$E(\xi)=-\beta^{-1}\ln\mathrm{Tr}(e^{-\beta H(\xi)})-\tfrac{1}{4}\sum_i(\tilde{U}_i\xi_i^2-\tilde{J}_i\xi_i^2)\ . \tag{2.3}$$

Here $\tilde{U}_i$ is an effective Coulomb integral defined by

$$\tilde{U}_i=\left[1-\frac{1}{2D}\right]U_i+\frac{1}{2D}J_i\ . \tag{2.4}$$

ζ_i in the Gaussian term is an average electron number with respect to $H(\xi)$.

The one-electron Hamiltonian $H(\xi)$ in Eq. (2.3) is expressed as

$$H(\xi)=\sum_{i\sigma}(\epsilon_i^0-\mu+\tfrac{1}{2}\tilde{U}_i\zeta_i-\tfrac{1}{2}\tilde{J}_i\xi_i\sigma-h_i\sigma)n_{i\sigma}+\sum_{ivjv'\sigma}t_{ivjv'}a_{iv\sigma}^{\dagger}a_{jv'\sigma}\ . \tag{2.5}$$

Here ϵ_i^0 and h_i are the atomic level and external magnetic field on site i, respectively. μ is the chemical potential. $t_{ivjv'}$ denotes the transfer integral between (site i, orbital v) and (site j, orbital v'). $a_{iv\sigma}^{\dagger}$ ($a_{iv\sigma}$) is the creation (annihilation) operator for electrons with spin σ on site i and orbital v. Furthermore, $n_{i\sigma}\equiv\sum_v a_{iv\sigma}^{\dagger}a_{iv\sigma}$.

The thermal average of the LM on site i is given by

$$\langle m_i\rangle=\langle\xi_i\rangle\ , \tag{2.6}$$

and the amplitude of the LM is given as follows [see Eqs. (3.15) and (3.24) in Ref. 34]:

$$\langle \mathbf{m}_i^2 \rangle = 3\langle \zeta_i \rangle - \frac{3}{2D}\langle \zeta_i^2 \rangle + \left[1+\frac{1}{2D}\right]\left[\langle \xi_i^2 \rangle - \frac{2}{\beta \tilde{J}_i}\right] . \tag{2.7}$$

Here $\langle \cdots \rangle$ in the right-hand side (rhs) means a classical average with respect to $E(\xi)$; that is, for a quantity X,

$$\langle X \rangle \equiv \frac{\int \left[\prod_i d\xi_i\right] X e^{-\beta E(\xi)}}{\int \left[\prod_i d\xi_i\right] e^{-\beta E(\xi)}} . \tag{2.8}$$

The new expression (2.7) for the amplitude of LM which takes account of the quantum effect has quite recently been derived from the free energy (2.1).[34] The well known formula for the amplitude of LM ($\langle \xi_i^2 \rangle - 2/\beta \tilde{J}_i$) by Wang *et al.*[36] leads neither to correct atomic limit nor to correct delocalized limit. It is also inconsistent with the free energy (2.1).

According to Hubbard[14] we consider a limit $\tilde{U} \to \infty$ and introduce charge potentials $\{w_i(\xi)\}$. These potentials are determined by the charge neutrality condition. Furthermore, we assume that the transfer integral can be expressed by a geometrical average: $t_{i\nu j\nu'} \equiv r_{i\nu}^* t^0_{i\nu j\nu'} r_{j\nu'}$, where $t^0_{i\nu j\nu'}$ is the transfer integral for a pure metal, and $r_{i\nu}$ is an off-diagonal factor which depends on a type of atom on site i.[37] Then Eq. (2.3) is written as follows (see Appendix for the derivation):

$$E(\xi) = \int d\omega f(\omega) \frac{1}{\pi} \mathrm{Im}\, \mathrm{Tr}[\ln(L^{-1} - t^0)] + \sum_i [-n_i w_i(\xi) + \tfrac{1}{4}\tilde{J}_i \xi_i^2] . \tag{2.9}$$

Here $f(\omega)$ is the Fermi distribution function. t^0 denotes the matrix $t^0_{i\nu j\nu'}$. n_i is the electron number on site i. The locator L is defined by

$$(L^{-1})_{i\nu j\nu'\sigma} = \frac{(\omega - \epsilon_i^0 - w_i(\xi) + \frac{1}{2}\tilde{J}_i \xi_i \sigma + \mu)}{|r_{i\nu}|^2} \delta_{ij}\delta_{\nu\nu'} . \tag{2.10}$$

It describes an atomic state with random potentials and exchange fields.

At finite temperatures the integration with respect to the exchange fields $\{\xi_i\}$ in Eqs. (2.1), (2.6), and (2.7) is not an easy task because the exchange fields couple each other via the first term at the right-hand side of the energy functional (2.9). Furthermore the evaluation of the latter itself is difficult in disordered alloys because of the existence of random potentials in the locator L. Thus we replace L^{-1} in Eq. (2.9) by an effective medium $\{\mathcal{L}^{-1}_{i\nu\sigma}\}$, which describes thermally and configurationally averaged states, and expand the deviation $\ln[1+(L^{-1} - \mathcal{L}^{-1})(\mathcal{L}^{-1} - t^0)^{-1}]$ with respect to the site.[38] The zeroth order is described by the effective medium only. The first-order correction consists of the sum of the single-site energy functionals $\{E_i(\xi_i)\}$,

$$E_i(\xi_i) = \int d\omega f(\omega) \frac{1}{\pi} \mathrm{Im} \sum_\nu^D \ln(L^{-1}_{i\nu\sigma} - \mathcal{L}^{-1}_{i\nu\sigma} + F^{-1}_{i\nu\sigma}) , \tag{2.11}$$

$$F_{i\nu\sigma} \equiv [(\mathcal{L}^{-1} - t^0)^{-1}]_{i\nu i\nu\sigma} . \tag{2.12}$$

In the next term the pair interaction terms $\sum_{(ij)} \Phi_{ij}(\xi_i, \xi_j)$ appear. $\Phi_{ij}(\xi_i, \xi_j)$ denotes the pair energy functional between sites i and j.

$$\Phi_{ij}(\xi_i, \xi_j) = \int d\omega f(\omega) \frac{1}{\pi} \mathrm{Im} \ln \det{}^{(ij)}(1 + \tilde{t}F') . \tag{2.13}$$

Here $\det^{(ij)}$ means the determinant of a 4D×4D matrix in the (i,j) subspace. $\tilde{t}$ and F' are the single-site t matrix and the off-diagonal coherent Green's function defined as follows:

$$(\tilde{t})_{i\nu j\nu'\sigma} = \frac{(L^{-1}_{i\nu\sigma} - \mathcal{L}^{-1}_{i\nu\sigma})}{1 + (L^{-1}_{i\nu\sigma} - \mathcal{L}^{-1}_{i\nu\sigma}) F_{i\nu\sigma}} \delta_{ij}\delta_{\nu\nu'} , \tag{2.14}$$

$$(F')_{i\nu j\nu'\sigma} = [(\mathcal{L}^{-1} - t^0)^{-1}]_{i\nu j\nu'\sigma}(1 - \delta_{ij}) . \tag{2.15}$$

All higher-order terms are neglected in the present theory by assuming small deviation from the effective medium. (See Ref. 20 for discussions on the validity of the approximation in alloys.) Then the energy functional $E(\xi)$ in Eqs. (2.1) and (2.6) is expressed as follows:

$$E(\xi) = \sum_i E_i(\xi_i) + \sum_{(ij)} \Phi_{ij}(\xi_i, \xi_j) . \tag{2.16}$$

Here we have omitted the zeroth term for brevity which does not make any contribution to the thermal averages (2.6) and (2.7).

The effective medium is determined so that the single-site t matrix (2.14) vanishes in average,

$$\langle |r_{i\nu}|^2 G_{i\nu\sigma}(\omega, \xi_i) \rangle = F_{i\nu\sigma}(\mathcal{L}^{-1}) \tag{2.17}$$

$G_{i\nu\sigma}(\omega, \xi_i)$ is the one-electron Green's function for orbital ν and spin σ at an impurity site i as defined by

$$G_{i\nu\alpha}(\omega, \xi_i) = \frac{1}{|r_{i\nu}|^2} (L^{-1}_{i\nu\sigma} - \mathcal{L}^{-1}_{i\nu\sigma} + F^{-1}_{i\nu\sigma})^{-1} . \tag{2.18}$$

Since the integration in the thermal average on the rhs of Eq. (2.6) is formidable, we replace the exchange-field variables $\{\xi_i\}$ except for the central site by the Ising spins making use of a following decoupling approximation which is correct up to the second moment:

$$\langle \xi_i^{2n+k} \rangle_0 \approx x_i^{2n} \langle \xi_i \rangle_0^k \quad (k = 0, 1) , \tag{2.19}$$

where

$$\langle \xi_i^k \rangle_0 \equiv \int d\xi_i (\xi_i^k) \exp[-\beta E_i(\xi_i)] / \int d\xi_i \exp[-\beta E_i(\xi_i)] ,$$

and similarly for ξ_i^{2n+k} and $x_i^2 \equiv \langle \xi_i^2 \rangle_0$. Then we have[10,38]

$$\langle m_0\rangle=\frac{\sum_{\{s\}}\int d\xi_0\xi_0 e^{-\beta\Psi'(\xi_0,s_1x_1,s_2x_2,\cdots)}}{\sum_{\{s\}}\int d\xi_0 e^{-\beta\Psi'(\xi_0,s_1x_1,s_2x_2,\cdots)}}\ , \tag{2.20}$$

$$\Psi'(\xi_0,s_1x_1,s_2x_2,\cdots)=E_0(\xi_0)+\sum_{i\neq0}\bar{\Phi}_{0i}(\xi_0)-\sum_{i\neq0}\left[\Phi^{\rm ex}_{0i}(\xi_0)+\beta^{-1}\tanh^{-1}\left[\frac{\langle\xi_i\rangle_0}{x_i}\right]+\sum_{j\neq0,i}\mathcal{H}_{ij}\right]s_i-\sum'_{(i,j)}\mathcal{J}_{ij}s_is_j\ . \tag{2.21}$$

Here $\sum_{\{s\}}$ means $\sum_{s_1}\sum_{s_2}\cdots$. $\sum'_{(i,j)}$ implies a summation with respect to all pairs which are not related to the site 0. Pair interactions $\bar{\Phi}_{0i}(\xi_0)$, $\Phi^{\rm ex}_{0i}(\xi_0)$, $\mathcal{H}_{ij}$, and $\mathcal{J}_{ij}$ are defined, respectively, as

$$\begin{bmatrix}\bar{\Phi}_{0i}(\xi_0)\\ \Phi^{\rm ex}_{0i}(\xi_0)\end{bmatrix}=\tfrac{1}{2}\sum_{\nu=\pm}\begin{bmatrix}1\\ \nu\end{bmatrix}\Phi_{0i}(\xi_0,\nu x_i)\ , \tag{2.22}$$

$$\begin{bmatrix}\mathcal{H}_{ij}\\ \mathcal{J}_{ij}\end{bmatrix}=-\tfrac{1}{4}\sum_{\lambda=\pm}\sum_{\nu=\pm}\lambda\begin{bmatrix}1\\ \nu\end{bmatrix}\Phi_{ij}(\lambda x_i,\nu x_j)\ . \tag{2.23}$$

The coupling $\mathcal{J}_{ij}$ means the exchange coupling between the atoms on site i and j as seen from the last term of the rhs in Eq. (2.21).

In the following, we make a molecular field approximation. Extension to the Bethe approximation is trivial.[10,18] In the molecular-field approximation the variables $\{s_i\}$ in Eq. (2.21) are replaced by their thermal averages: $\langle s_i\rangle=\langle m_i\rangle/x_i$. Equations (2.20) and (2.21) then reduce to

$$\langle m_i\rangle(\{\gamma_i\},\{\langle m_i\rangle\})=\frac{\int d\xi\,\xi e^{-\beta\Psi(\xi)}}{\int d\xi e^{-\beta\Psi(\xi)}}\ , \tag{2.24}$$

$$\Psi(\xi)=E_0(\xi)+\sum_{i\neq0}\bar{\Phi}_{0i}(\xi)-\sum_{i\neq0}\Phi^{\rm ex}_{0i}(\xi)\frac{\langle m_i\rangle}{x_i}\ . \tag{2.25}$$

Here γ_i denotes a type of atom on site i.

A local magnetic moment depends on the surrounding atomic and magnetic configurations $\{\gamma_i\}$ and $\{\langle m_i\rangle\}$ via the energy functional $\Psi(\xi)$. Therefore the LM's have a distribution due to the randomness. When a binary alloy is ferromagnetic the effective medium $\mathcal{L}^{-1}_{i\nu\sigma}$ may be independent of site i. Then the distribution function of LM of atom α depends on the type α only, which we write as $g^{(1)}_\alpha(M)$. When the alloy forms the antiferromagnetic state with two sublattices ($+$ and $-$) we have to introduce two kinds of effective medium $\{\mathcal{L}^{(\pm)}_{\nu\sigma}\}$ depending on whether the site belongs to ($+$) or ($-$) sublattice. Thus we have four kinds of distribution functions $g^{(1\pm)}_\alpha(M)$. However there are symmetry relations between the ($+$) and ($-$), e.g., $\mathcal{L}^{(-)}_{\nu\sigma}=\mathcal{L}^{(+)}_{\nu-\sigma}$ and $g^{(1-)}_\alpha(M)=g^{(1+)}_\alpha(-M)$. Thus we can proceed by using the quantities on sublattice ($+$) only. We omit ($+$) sign in the following promising that $\mathcal{L}_{\nu\sigma}\equiv\mathcal{L}^{(+)}_{\nu\sigma}$, $g^{(1)}_\alpha(M)\equiv g^{(1+)}_\alpha(M)$, etc.

The LM's $\{\langle m_i\rangle\}$ which determine the central LM $\langle m_0\rangle$ are also determined by their surrounding LM's. They should have the same distribution functions as in the central site. This leads to an integral equation for $g^{(1)}_\alpha(M)$ (see Ref. 17 and Appendix in Ref. 20),

$$g^{(1)}_\alpha(M)=\sum_{\gamma_1}\cdots\sum_{\gamma_z}\int\delta(M-\langle m_0\rangle(\{\gamma_i\},\{m_i\}))\times\prod_i^z[p_a^{\alpha\gamma_i}g^{(1)}_{\gamma_i}(\pm m_i)dm_i]\ . \tag{2.26}$$

Here the upper (lower) sign in $g^{(1)}_{\gamma_i}$ at the rhs is for the ferromagnetic (antiferromagnetic) state. We have only taken into account the nearest-neighbor (NN) pair interactions. z is the number of NN's. $p_a^{\alpha\gamma}$ is the probability of finding atom γ at a neighboring site of atom α. It is given by Cowley's atomic short-range order parameter[39] τ as $p_a^{\alpha\gamma}=c_\gamma+(\delta_{\alpha\gamma}-c_\gamma)\tau$, c_γ being the concentration of atom γ.

It is difficult to find the solution of integral equation (2.26) for bcc ($z=8$) and fcc ($z=12$) without further approximation. We make a decoupling approximation in the rhs;

$$\int M^{2n+k}g^{(1)}_\alpha(M)dM\approx(x_\alpha v_\alpha)^{2n}(x_\alpha u_\alpha)^k\quad(k=0,1) \tag{2.27}$$

and

$$x_\alpha u_\alpha\equiv[\langle m_\alpha\rangle]_c=\int Mg^{(1)}_\alpha(M)dM\ , \tag{2.28}$$

$$x_\alpha^2v_\alpha^2\equiv[\langle m_\alpha\rangle^2]_c=\int M^2g^{(1)}_\alpha(M)dM\ , \tag{2.29}$$

where $[\cdots]_c$ denotes the configurational average. The approximation is correct up to the second moment. It may be more reasonable for the system with a larger number of z. Then Eq. (2.26) reduces to

$$g^{(1)}_\alpha(M)=\sum_{n=0}^{z}\Gamma(n,z,p_a^{\alpha\alpha})\sum_{k=0}^{n}\sum_{l=0}^{z-n}\Gamma(k,n,q_{\alpha+})\Gamma(l,z-n,q_{\bar{\alpha}+})\delta(M-\langle\xi_\alpha\rangle_{nkl})\ . \tag{2.30}$$

Here $\Gamma(n,z,p_a^{\alpha\alpha})$ is the binomial distribution function,

$$\frac{z!}{n!(z-n)!}(p_a^{\alpha\alpha})^n(1-p_a^{\alpha\alpha})^{z-n}\ . \tag{2.31}$$

$q_{\alpha+}$ in Eq. (2.30) is defined by

$$q_{\alpha+}=\frac{1}{2}\left[1+\frac{u_\alpha}{v_\alpha}\right]\ . \tag{2.32}$$

This is interpreted as the probability that the fictitious spin on atom α with magnitude v_α is in the up direction.

The quantity $\langle \xi_\alpha \rangle_{nkl}$ in Eq. (2.30) is the LM of an atom of type α when k of the fictitious spins among the surrounding n atoms of type α point up, and l spins of the remaining $z-n$ atoms of type $\bar{\alpha}$ also point up.

$$\langle \xi_\alpha \rangle_{nkl} = \int p_{\alpha nkl}(\xi)\xi \, d\xi \ , \tag{2.33}$$

$$p_{\alpha nkl}(\xi) = \frac{e^{-\beta\Psi_{\alpha nkl}(\xi)}}{\int d\xi \, e^{-\beta\Psi_{\alpha nkl}(\xi)}} \ , \tag{2.34}$$

$$\Psi_{\alpha nkl}(\xi) = E_\alpha(\xi) + n\bar{\Phi}_{\alpha\alpha}(\xi) + (z-n)\bar{\Phi}_{\alpha\bar{\alpha}}(\xi) \mp (2k-n)\Phi^{\rm ex}_{\alpha\alpha}(\xi)v_\alpha \mp (2l-z+n)\Phi^{\rm ex}_{\alpha\bar{\alpha}}v_{\bar{\alpha}} \ . \tag{2.35}$$

Here we have replaced the site index (i) by the type (α) of atom on the same site.

Substituting Eq. (2.30) into Eqs. (2.28) and (2.29) we obtain the self-consistent equations to determine u_α and v_α:

$$x_\alpha u_\alpha = [\langle m_\alpha \rangle]_c \ , \tag{2.36}$$

$$x_\alpha^2 v_\alpha^2 = [\langle m_\alpha \rangle^2]_c \ , \tag{2.37}$$

$$[\langle m_\alpha \rangle^i]_c \equiv \sum_{n=0}^{z} \Gamma(n,z,p_a^{\alpha\alpha})[\langle m_\alpha \rangle_n^i]_c \quad (i=1,2) \ , \tag{2.38}$$

$$[\langle m_\alpha \rangle_n^i]_c \equiv \sum_{k=0}^{n}\sum_{l=0}^{z-n} \Gamma(k,n,q_{\alpha+}) \times \Gamma(l,z-n,q_{\bar{\alpha}+})(\langle \xi_\alpha \rangle_{nkl})^i \ . \tag{2.39}$$

The same consideration for Eq. (2.17) leads to a simplified CPA equation,

$$\sum_\alpha c_\alpha \sum_{\nu=\pm} \frac{1}{2}\left[1+\nu\frac{[\langle \xi_\alpha \rangle]_c}{([\langle \xi_\alpha^2 \rangle]_c)^{1/2}}\right] |r_{\alpha\nu}|^2 G_{\alpha\nu\sigma}\{\omega,\nu([\langle \xi_\alpha^2 \rangle]_c)^{1/2}\} = F_{\nu\sigma} \ , \tag{2.40}$$

$$[\langle \xi_\alpha^i \rangle]_c = \sum_{n=0}^{z} \Gamma(n,z,p_a^{\alpha\alpha}) \sum_{k=0}^{n}\sum_{l=0}^{z-n} \Gamma(k,n,q_{\alpha+})\Gamma(l,z-n,q_{\bar{\alpha}+})\langle \xi_\alpha^i \rangle_{nkl} \ , \tag{2.41}$$

$$\langle \xi_\alpha^i \rangle_{nkl} = \int p_{\alpha nkl}(\xi)\xi^i d\xi \ , \tag{2.42}$$

where $i=0,1$.

Solving Eqs. (2.36), (2.37), and (2.40) self-consistently, we obtain u_α, v_α, and $\mathcal{L}_{\nu\sigma}$. The charge potential $\epsilon_\alpha^0 + w_\alpha(\xi) - \mu$ in $E_\alpha(\xi)$ and $\Phi_{\alpha\gamma}(\xi)$ is determined by the charge neutrality condition on a site.

The amplitude distribution function is obtained as follows by using the same approximation scheme as in the derivation of Eq. (2.30) (see the Appendix in Ref. 20):

$$g_\alpha^{(2)}(M) = \sum_{n=0}^{z} \Gamma(n,z,p_a^{\alpha\alpha}) \sum_{k=0}^{n}\sum_{l=0}^{z-n} \Gamma(k,n,q_{\alpha+})\Gamma(l,z-n,q_{\bar{\alpha}+})\delta(M-(\langle \mathbf{m}_\alpha^2 \rangle_{nkl})^{1/2}) \ , \tag{2.43}$$

$$\langle \mathbf{m}_\alpha^2 \rangle_{nkl} \equiv 3n_\alpha - \frac{3}{2D}n_\alpha^2 + \left[1+\frac{1}{2D}\right]\left[\langle \xi_\alpha^2 \rangle_{nkl} - \frac{2}{\beta\bar{J}_\alpha}\right] \ . \tag{2.44}$$

Here the site indices have been replaced by the types of atoms.

The internal field H_i seen by atom α at site i is assumed to follow a phenomenological expression,[40]

$$H_i = a_\alpha \langle m_i \rangle + \sum_{l=1}^{2}\sum_{j=1}^{z_l} b_{\alpha\gamma_j}^{(l)} \langle m_j \rangle \ . \tag{2.45}$$

Here z_l is the number of the lth NN sites. $\langle m_j \rangle$ is the average LM at the lth NN site j. a_α and $b_{\alpha\gamma_j}^{(l)}$ are the proportionality constants. Then the internal-field distribution function $P_\alpha(H)$ for atom α is given in the molecular-field approximation as follows:[20]

$$P_\alpha(H) = \sum_{n_1}\sum_{n_2} \Gamma(n_1,z_1,p_1^{\alpha\alpha})\Gamma(n_2,n_2,p_2^{\alpha\alpha}) \times \sum_{k_1}^{n_1}\sum_{k_2}^{n_2}\sum_{m_1}^{z_1-n_1}\sum_{m_2}^{z_2-n_2} \Gamma(k_1,n_1,q_{\alpha+})\Gamma(k_2,n_2,q_{\alpha+}) \times \Gamma(m_1,z_1-n_1,q_{\bar{\alpha}+})\Gamma(m_2,z_2-n_2,q_{\bar{\alpha}+})\delta(H-H_\alpha(\{n_l\},\{k_l\},\{m_l\})) \ . \tag{2.46}$$

$$H_\alpha(\{n_l\},\{k_l\},\{m_l\}) = a_\alpha\langle \xi_\alpha \rangle_{nkl} \pm \sum_{l=1}^{2}[b_{\alpha\alpha}^{(l)}(2k_l-n_l)x_\alpha v_\alpha + b_{\alpha\bar{\alpha}}^{(l)}(2m_l-z_l+n_l)x_{\bar{\alpha}}v_{\bar{\alpha}}] \ . \tag{2.47}$$

Here $p_l^{\alpha\alpha}$ is the probability of finding an atom of type α at the lth NN when the central site is occupied by atom α. Note that $z_l=z$ and $p_l^{\alpha\alpha}=p_a^{\alpha\alpha}$. Internal-field distribution function in the antiferromagnetic alloys should be given by $[P_\alpha(H)+P_\alpha(-H)]$, because Eq. (2.46) is for $(+)$ sublattice. All results for $g_\alpha^{(1)}(M)$, $g_\alpha^{(2)}(M)$, and $P_\alpha(H)$ will be given by a histogram in the following sections.

III. NUMERICAL CALCULATIONS AND PARAMETERS

In the numerical calculations we adopted the fivefold equivalent band model which greatly reduces the computing time:

$$H(\xi)=\sum_\nu \left[\sum_{i\sigma} [\epsilon_i^0-\mu+w_i(\xi)-\tfrac{1}{2}\tilde{J}_i\xi_i\sigma-h_i\sigma] \times n_{i\nu\sigma}+\sum_{ij\sigma} t_{ij}a_{i\nu\sigma}^\dagger a_{j\nu\sigma} \right] . \tag{3.1}$$

The model is suitable for a qualitative or semiquantitative description, and includes the effect of degeneracy and Hund's rule coupling.[34]

The orbital dependence drops in all the equations in the previous section when we use the Hamiltonian (3.1). The coherent Green's function (2.12) is then expressed for ferromagnetic state as

$$F_\sigma=\int \frac{\rho_0(\epsilon)d\epsilon}{\mathcal{L}_\sigma^{-1}-\epsilon} , \tag{3.2}$$

where $\rho_0(\epsilon)$ is the density of states (DOS) for a pure metal $\{t_{ij}^0\}$. In the antiferromagnetic case we use further approximation $\epsilon_{k+Q}=-\epsilon_k$ for the dispersion curves to $\{t_{ij}^0\}$, Q being $2\pi(1,0,0)/a$ in the case of the bcc lattice where a denotes the lattice parameter of the unit cell. The relation $\epsilon_{k+Q}=-\epsilon_k$ holds true when the NN transfer integrals are only taken into account. Equation (2.12) then reduces to a simplified expression as follows:[41,42]

$$F_\sigma=\left[\frac{\mathcal{L}_{-\sigma}(\omega)}{\mathcal{L}_\sigma(\omega)}\right]^{1/2}\int \frac{\rho_0(\epsilon)d\epsilon}{[\mathcal{L}_+(\omega)\mathcal{L}_-(\omega)]^{1/2}-\epsilon} . \tag{3.3}$$

Input parameters used in the calculation are d electron number n_α, d band width W_α, effective exchange parameter $\tilde{J}_\alpha$, and the model DOS, $\rho_0(\epsilon)$. The latter is given in the inset of Fig. 1. Others are chosen as follow:

$$n_{\mathrm{Fe}}=7.00,\quad W_{\mathrm{Fe}}=0.45\ \mathrm{Ry},\quad \tilde{J}_{\mathrm{Fe}}=0.0697\ \mathrm{Ry} .$$

$$n_{\mathrm{Cr}}=4.72,\quad W_{\mathrm{Cr}}=0.58\ \mathrm{Ry},\quad \tilde{J}_{\mathrm{Cr}}=0.0350\ \mathrm{Ry} .$$

Parameters for Fe are the same as in the Fe-V alloys.[20,43] The d-band width for Cr is taken from Kübler's calculations.[44] n_{Cr} and W_{Cr} are chosen so that (i) the Fermi level of pure Cr is in the dip of the DOS which arises from the nesting part in the antiferromagnetic energy dispersion curves, (ii) the sublattice magnetization is about $0.6\mu_B$ at the ground state.[45,46]

The numerical calculations have been done above 75 K because of the difficulties of integration with respect to the energy ω and field variable ξ. The results are extrapolated to the zero temperature.

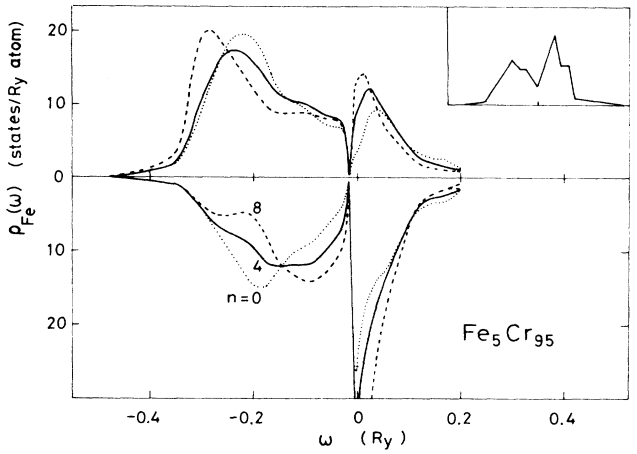

FIG. 1. Local density of states for Fe in various environments in the antiferromagnetic state. Here and in the following figures the environments are specified by n, the number of Fe nearest neighbors (NN's). The inset shows the model density of states used in the present calculations.

A typical example of the DOS in various environments in the antiferromagnetic state is shown in Fig. 1. The model DOS $\rho_0(\epsilon)$ in the inset has been used in the previous calculations for the bcc metals and alloys.[20,35,47] A sharp dip is seen near the Fermi level, which is due to the use of the perfect nesting relation $\epsilon_{k+Q}=-\epsilon_k$. The difference in line shapes of the local DOS is mainly determined by the average atomic levels for up and down spins in each environment.

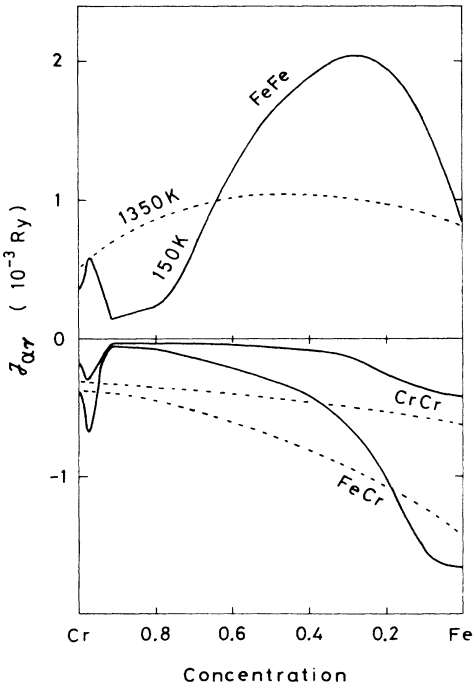

FIG. 2. Concentration dependence of effective pair energies $\mathcal{J}_{\alpha\gamma}$ at 150 K (solid curves) and 1350 K (dashed curves).

IV. PHASE DIAGRAM

Rough features of the magnetism of Fe-Cr alloys can be understood by means of the nearest-neighbor exchange interactions $\{\mathcal{J}_{\alpha\gamma}\}$. They are shown in Fig. 2. The coupling between Fe LM's is ferromagnetic, while the coupling between Cr LM's is antiferromagnetic. This explains the ferromagnetism in Fe-rich concentrations and the antiferromagnetism in Cr-rich concentrations. The antiferromagnetic coupling between Cr and Fe LM's implies that Cr LM's are antiparallel to the bulk magnetization in the ferromagnetic state. There is no frustration of the magnetic arrangement until the number of the antiferromagnetic Cr-Cr pairs becomes comparable to that of the Cr-Fe pairs.

The calculated phase diagram is shown in Fig. 3 together with the experimental one. The present theory describes qualitatively the experimental phase diagram.[21] A maximum of T_C around 5 at. % Fe (15 at. % Fe in our calculation) is explained by the enhancement of the Fe-Fe coupling $\mathcal{J}_{\mathrm{FeFe}}$ as shown in Fig. 2. This is an alloying effect due to the band mixing, which is not explained by the rigid band model.[48] The same situation has been found in Fe-V alloys.[20]

The present calculations give the Néel temperature of pure Cr higher than the experimental value[49] (310 K). This is because of the use of a simplified expression (3.3) for the coherent Green's function. Note that Eq. (3.3) was derived by assuming a symmetric band which produces a completely nesting Fermi surface for the half-filled case. The antiferromagnetic energy is overestimated for this reason. One has to take the antiferromagnetic band structure into account more seriously for quantitative discussion.

It has been suggested in the experimental investigations[21,22] that the spin-glass state exists in a small concentration range (81–84 at. % Cr) at temperatures less than 30 K. Theoretically Jo claimed that the spin-glass state was possible on the basis of simple CPA calculations.[33] It is not accepted, however, because there is no order parameter to distinguish the spin-glass state from the paramagnetic state in simple CPA calculations. In the present theory the spin-glass solution ($[\langle m_\alpha\rangle^2]_c\neq 0$ and $[\langle m\rangle]_c=0$) is clearly distinguished from the paramagnetic solution ($[\langle m_\alpha\rangle^2]_c=[\langle m\rangle]_c=0$), but it does not appear above 75 K according to the numerical calculations. When the temperature decreases the Cr LM lose the exchange splitting, therefore the antiferromagnetic Cr-Cr and Cr-Fe couplings disappear. The remaining Fe-Fe NN coupling is ferromagnetic. Thus we do not expect the spin-glass solution at the ground state. We have to take account of more distant pair interactions to obtain the spin-glass solution. In what follows we assume that LEE due to long-range interactions which cause the spin-glass solution at low temperatures are not important at higher temperatures ($\gtrsim 100$ K). This is reasonable because the random configurations of thermally induced LM's cause the damping of pair interactions.[50,51]

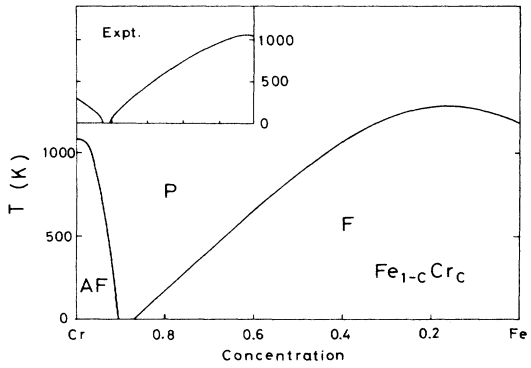

FIG. 3. Calculated magnetic phase diagram of Fe-Cr alloys and the experiment (inset) (Refs. 21, 23, and 29). F, P, and AF mean the ferromagnetic state, and paramagnetic state, and the antiferromagnetic state, respectively.

V. CONCENTRATION DEPENDENCE

The magnetization and average LM of constituent atoms change monotonically as shown in Fig. 4, and disappear at 80 at. % Cr. The results are consistent with the neutron experiments as well as previous CPA calcula-

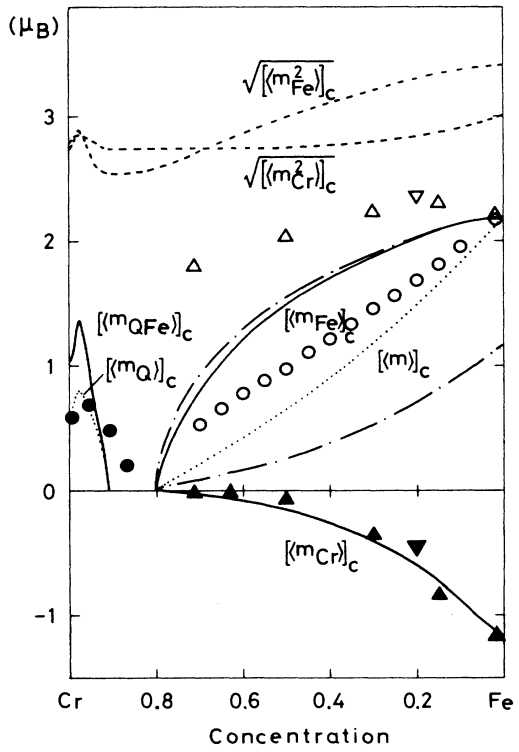

FIG. 4. Concentration dependences of the magnetization ($[\langle m\rangle]_c$), sublattice magnetization ($[\langle m_Q\rangle]_c$), and various local moments at 150 K. Experimental values are shown by open circles for magnetization (Ref. 52) closed circles for sublattice magnetization (Refs. 29, 45, and 46) and triangles for the average local moments of constituent atoms ($[\langle m_\alpha\rangle]_c$) (Refs. 53 and 54). The local moments $([\langle m_\alpha\rangle^2]_c)^{1/2}$ are also shown by dashed-dotted lines.

tions.[31,32] The sublattice magnetization in the antiferromagnetic state shows a peak near 2 at. % Fe. It is related to the position of the Fermi level in the gap of the DOS, and therefore it is considerably parameter dependent. Experimentally the alloy changes from a commensurate to an incommensurate spin-density-wave state near 2 at. % Fe with decreasing Fe concentration.[28,29] The fact that the maximum amplitude of the local magnetization in the incommensurate phase is smaller than that of the commensurate one seems to support the present result. The amplitudes of the LM calculated from our new formula (2.7) have large values as compared with the previous results for Fe-V alloys.[55] The enhancement of the Cr LM due to the quantum effect is much larger than that of Fe but the concentration dependence of the iron is stronger than the Cr because of larger change of $[\langle \xi^2_{\rm Fe} \rangle]_c$. Thus we see in Fig. 4 a crossing of the amplitude curves at 70 at. % Cr, which does not appear when the classical expression is adopted.

The LEE in the ferromagnetic state are more or less similar to those of Fe-V alloys[20] as shown in Fig. 5(a). The Fe LM's with larger number of Fe NN's have larger local magnetization. This is not due to the enhancement of the ferromagnetic exchange coupling with surrounding Fe LM's but due to the increase of an amplitude $\langle \xi^2_{\rm Fe} \rangle$. The latter is caused by the atomic pair energy $\bar{\Phi}_{\rm FeFe}(\xi)$ which shows a sharp upward convex curve as shown in Fig. 6. The Cr LM with no neighboring Cr LM is antiparallel to the magnetization as discussed in the previous section. When the number of neighboring Cr LM antiparallel to the magnetization increases, the Cr LM at the central site reverses as seen from Fig. 5(a). Calculated LM in the concentrated alloys show a broad distribution as shown in Fig. 7(a). Concentration dependence of the distribution functions is similar to the Fe-V alloys, but the line width of $g^{(1)}_{\rm Cr}(M)$ is larger than that of $g^{(1)}_{\rm V}(M)$ in Fe-V alloys because of stronger antiferromagnetic couplings $\mathcal{J}_{\rm CrCr}$.

Internal-field distribution functions created by the LM distributions are presented in Fig. 8. Theoretical curves at 150 K show a broad distribution in agreement with the experiments.[25] This justifies the existence of the LEE on the LM's. However the experimental linewidths are narrower than the theoretical ones. This is presumably due to the temperature effect. (The experimental curves are obtained at 4.2 K, while the theoretical ones are calculated at 150 K.) The temperature dependence of the distribution function is strong in particular near the critical concentration of the ferromagnetic instability. This is seen by comparing the experimental curves at 75 at. % Fe and 4.2 K in Fig. 8 with those in the inset of Fig. 12.

In the antiferromagnetic phase the LEE on Fe LM's changes its nature at 5 at. % Fe. The Fe LM with more than four Fe NN's couple antiferromagnetically to the surrounding Fe LM when the Fe concentration $c_{\rm Fe}$ is less than 5 at. % Fe. This is not explained by the sign of the simple exchange coupling $\mathcal{J}_{\rm FeFe}$ only. The local magnetization is determined by the single-site term $E_{\rm Fe}(\xi)$, the atomic pair functions $\bar{\Phi}_{\alpha\gamma}(\xi)$, and the exchange terms $\Phi^{\rm ex}_{\alpha\gamma}(\xi)$ [see Eq. (2.35)]. The single-site energy functional of Fe $[E_{\rm Fe}(\xi)]$ has a deep minimum at $\xi = 1\mu_B$ on the $(+)$ sublattice in the pure Cr metal, which is related to the gap of the DOS near the Fermi level. Therefore the nearest-neighbor exchange pair energy $\Phi^{\rm ex}_{\rm FeFe}(\xi)$ depicted in Fig. 6 cannot change the direction of Fe LM's even when the central Fe LM is surrounded by eight Fe LM's. The role of atomic pair energy $\bar{\Phi}_{\rm FeFe}(\xi)$ with strong convexity (see Fig. 6) shift the position of the minimum in

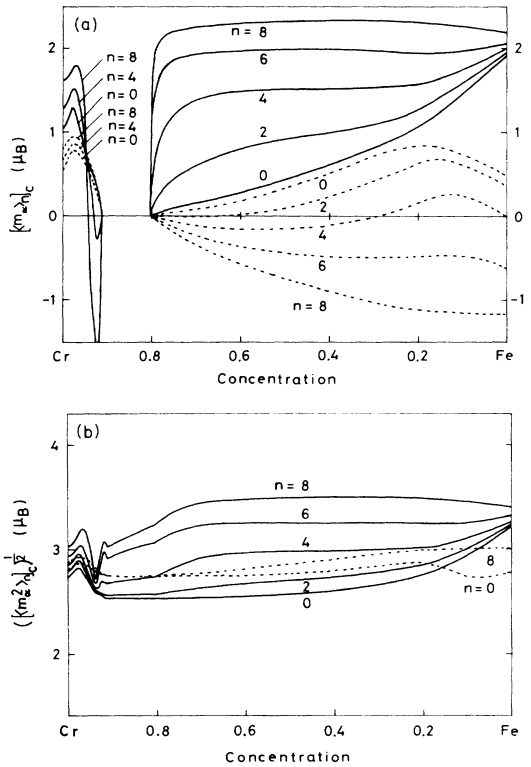

FIG. 5. Local magnetic moments in various environments for Fe (solid curves) and Cr (dashed curves): (a), $[\langle m_\alpha \rangle_n]_c$; (b), $([\langle \mathbf{m}^2_\alpha \rangle_n]_c)^{1/2}$.

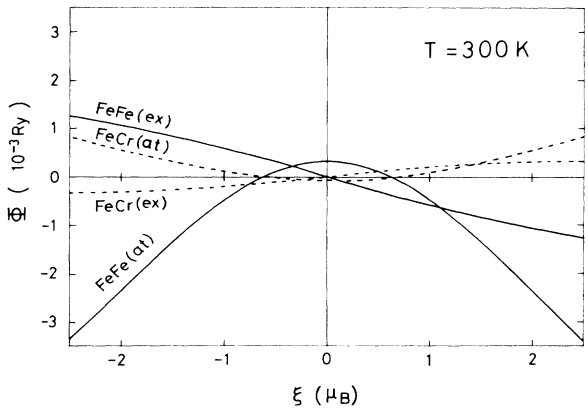

FIG. 6. Pair energy functionals $\bar{\Phi}_{\alpha\gamma}(\xi)$ and $-\Phi^{\rm ex}_{\alpha\gamma}(\xi)$ at 80 at. % Fe. The notation $\alpha\gamma$(at) $[\alpha\gamma$(ex)] means the former (the latter).

$\Psi(\xi)$ to a larger value in the low Fe concentrations. This is because the Fe LM coupled antiferromagnetically to the surrounding LM's increase with increasing number of Fe NN's. As seen from the mechanism mentioned above, the increase of Fe LM's does not mean the enhancement of the Fe-Fe antiferromagnetic coupling.

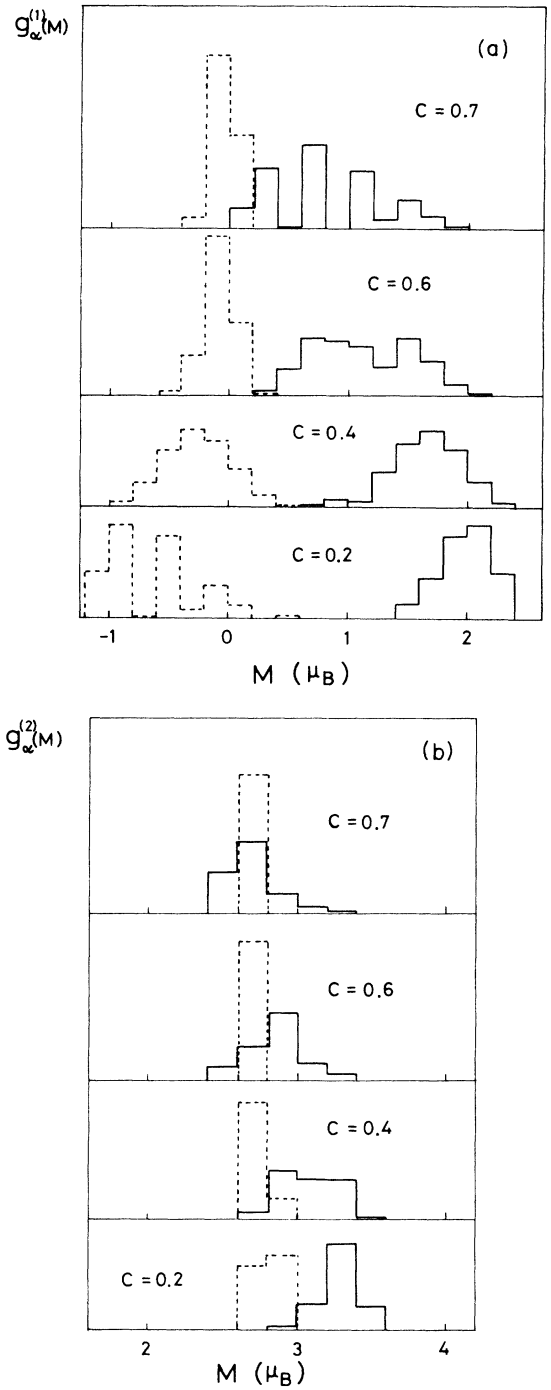

FIG. 7. Concentration dependence of the local-moment distribution for Fe (solid lines) and Cr (dashed lines) at $T=150$ K: (a), $g_\alpha^{(1)}(M)$; (b), $g_\alpha^{(2)}(M)$.

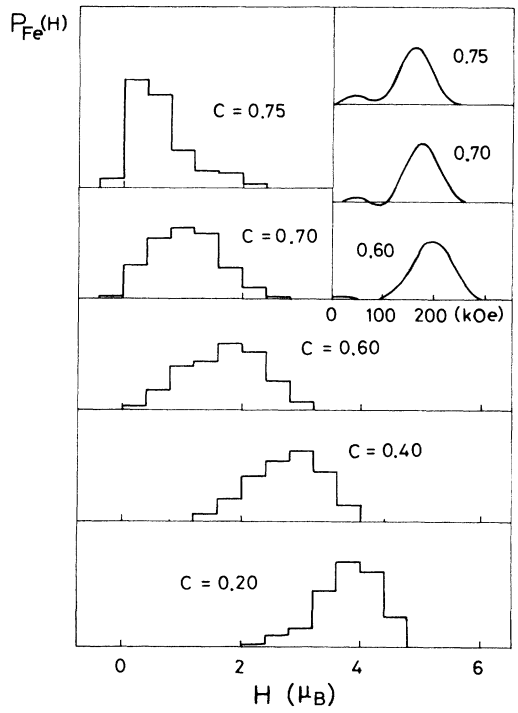

FIG. 8. Internal-field distribution seen by ^{57}Fe as a function of Cr concentration at $T=150$ K. The field H is measured in units of $a_{Fe}=1$. Parameters $b^{(1)}_{FeFe}/a_{Fe}=b^{(1)}_{FeCr}/a_{Fe}=0.090$ and $b^{(2)}_{FeFe}/a_{Fe}=b^{(2)}_{FeCr}/a_{Fe}=0.076$ are taken from Ref. 25. The inset shows the experimental results at 4.2 K by Shiga and Nakamura (Ref. 25).

When the Fe concentration increases the gap of the DOS disappears at about 5 at. % Fe. The minimum of the single-site energy $E_{Fe}(\xi)$ then becomes shallow. The ferromagnetic exchange energy $\Phi^{ex}_{FeFe}(\xi)$ becomes relatively important. Thus the reversal of Fe LM's with more than four Fe NN's takes place at about 5 at. % Fe in Fig. 5(a).

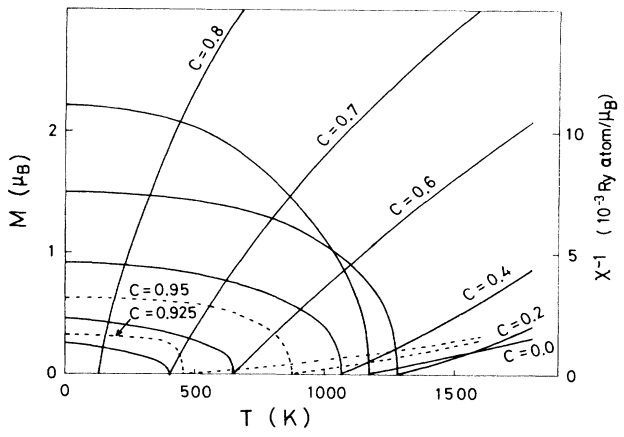

FIG. 9. Magnetization-vs-temperature curves and inverse susceptibilities in various Cr concentrations. Sublattice magnetization and the staggered susceptibilities are shown by dotted curves.

The LEE on the amplitude of LM is reduced by a factor of 2 when the quantum effect is taken into account. This is shown in Figs. 5(b) and 7(b). The change of the amplitude of Cr LM due to the LEE is generally small because of a weak ξ dependence of $\bar{\Phi}_{CrCr}(\xi)$ and $\bar{\Phi}_{CrFe}(\xi)$.

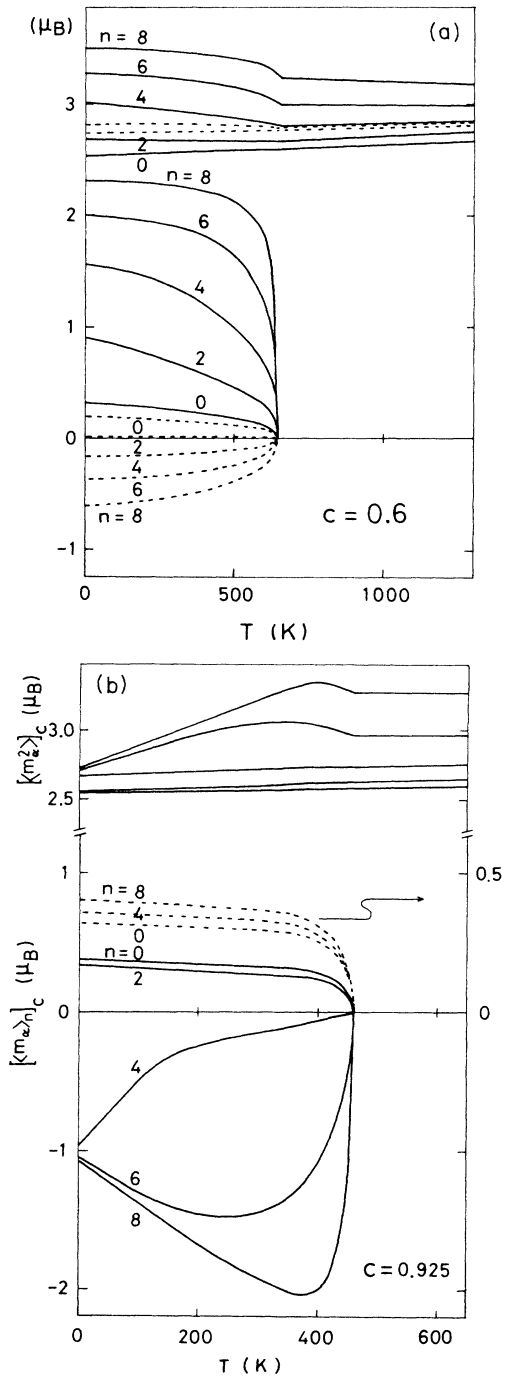

FIG. 10. Temperature dependence of average local moments $[\langle m_\alpha \rangle_n]_c$ and amplitudes $([\langle \mathbf{m}_\alpha^2 \rangle_n]_c)^{1/2}$ in various environments. Fe (Cr) parts are shown by solid curves (dashed curves). (a) Ferromagnetic state (60 at. % Cr). (b) Antiferromagnetic state (92.5 at. % Cr).

VI. TEMPERATURE VARIATIONS

The magnetization versus temperature curves are shown in Fig. 9. They are consistent with the previous results within the SSA.[8] The sublattice magnetization rapidly decreases near T_N. The reason is that the energy gain of the antiferromagnetic states rapidly decrease with the disappearance of the gap in the DOS. The temperature variations of LM with fixed number of Fe NN's in the ferromagnetic state are close to those in Fe-V alloys as shown in Fig. 10(a).

The temperature dependence of the amplitude of the LM's is suppressed by the quantum effect[35] as compared with the classical results $[(\langle \xi_\alpha^2 \rangle - 2/\beta \tilde{J}_\alpha)^{1/2}]$. Since weak and strong Fe LM's coexist in the concentrated alloys, we find in Fig. 10(b) an increasing amplitude $[\langle \mathbf{m}_{Fe}^2 \rangle_0]_c^{1/2}$ as well as a decreasing amplitude $[\langle \mathbf{m}_{Fe}^2 \rangle_8]_c^{1/2}$ when the temperature rises. In the lower Fe concentration, the Fe LM's are weaker than those of 60 at. % Fe in Fig. 10(a). Therefore they have relatively small amplitudes of LM at low temperatures. When the temperature is elevated in this situation the amplitude of exchange splitting x_{Fe} and therefore the coupling $\mathcal{J}_{FeFe}$ become larger. Then $[\langle \mathbf{m}_{Fe}^2 \rangle_8]_c^{1/2}$ and $|[\langle m_{Fe} \rangle_8]_c|$ are increased by the temperature induced x_{Fe} and the enhanced ferromagnetic coupling $\mathcal{J}_{FeFe}$.

The temperature dependence of the LM distribution and the internal field distribution is shown in Figs. 11 and 12. A shoulder at $H = 1.4\mu_B$ in the calculation of $P_{Fe}(H)$ at $T = 0.26T_C$ is consistent with the observed distributions by Dubiel *et al.*[26] which is in the inset of Fig. 12. This is produced by the polarization of surrounding Fe LM's as can be seen by comparing the spectra $P_{Fe}(H)$ in Fig. 12 with the distribution $g_{Fe}^{(1)}(M)$ in Fig. 11.

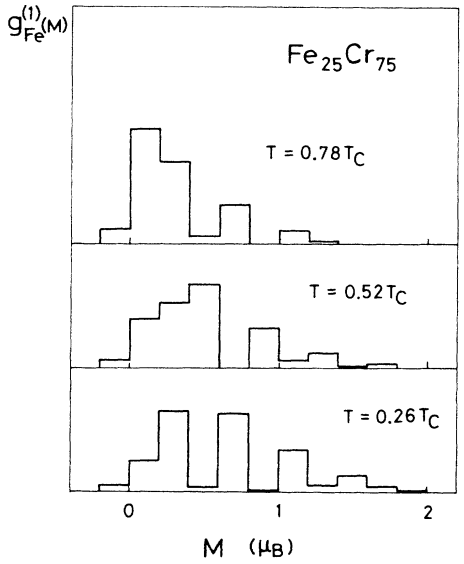

FIG. 11. Temperature variation of the distribution of Fe local moments at 75 at. % Cr.

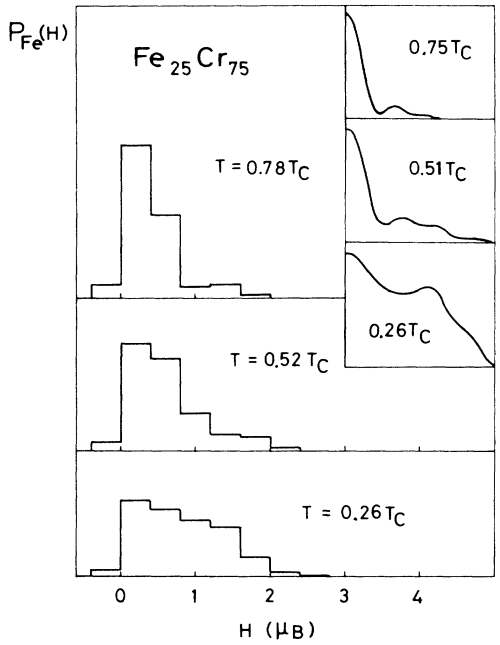

FIG. 12. Temperature variation of the internal field distribution for ^{57}Fe at 75 at.% Cr and the experimental results by Dübiel *et al.* (Ref. 26) (inset). Parameters $b^{(1)}_{\alpha\gamma}/a_\alpha$ are the same as in Fig. 8.

VII. SUSCEPTIBILITY

High-field susceptibilities (see Fig. 13) are calculated numerically by applying small uniform fields (0.000 05–0.0001 Ry in units of $g\mu_B/2$). The calculations in the antiferromagnetic regime have not yet been done because one has to perform the calculations of the ferrimagnetic states. The results which are shown in Fig. 11 explain the experiments[30] in the ferromagnetic regime, but they are too small in the spin-glass and antiferromagnetic states. This might be due to the temperature difference between the theory and the experiments (4.2 K). One expects a Curie-like behavior of Fe LM because of the existence of Fe LM in the infinitesimal molecular fields. Friedel and Hedmann[57] proposed a mechanism of the Curie-like behavior due to the ferromagnetically coupled Fe NN pairs in the antiferromagnetic Cr. If we assume the NN exchange interaction, one needs a condition $\mathcal{J}_{\mathrm{FeFe}} > 7\,|\,\mathcal{J}_{\mathrm{FeCr}}\,|$ to produce such ferromagnetically coupled Fe pairs. This condition is not plausible according to our calculation in Fig. 2. One has to take into consideration the LEE due to extended interactions to examine the validity of the model in more details.

Figure 14 shows the concentration dependence of the effective Bohr magneton number and the Weiss constant at high temperatures. They are calculated from the paramagnetic inverse spin susceptibilities in Fig. 9. The effective Bohr magneton numbers m_{eff} decrease with in-

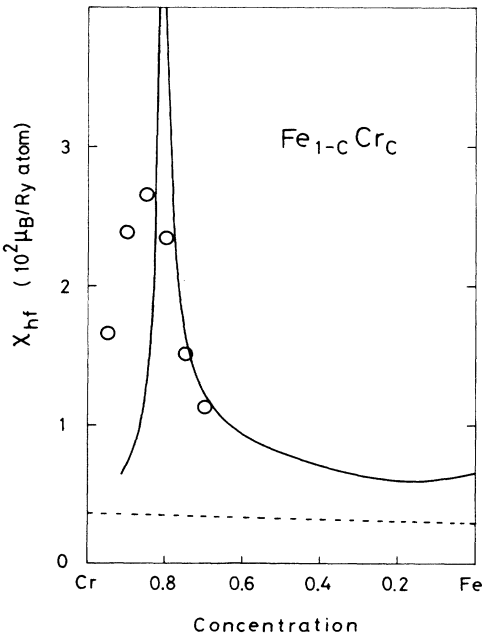

FIG. 13. High-field susceptibility as a function of the concentration. Orbital contribution (dashed line) (Ref. 56) has been added. Open circles show the experimental data by Cey and Kunitomi (Ref. 30).

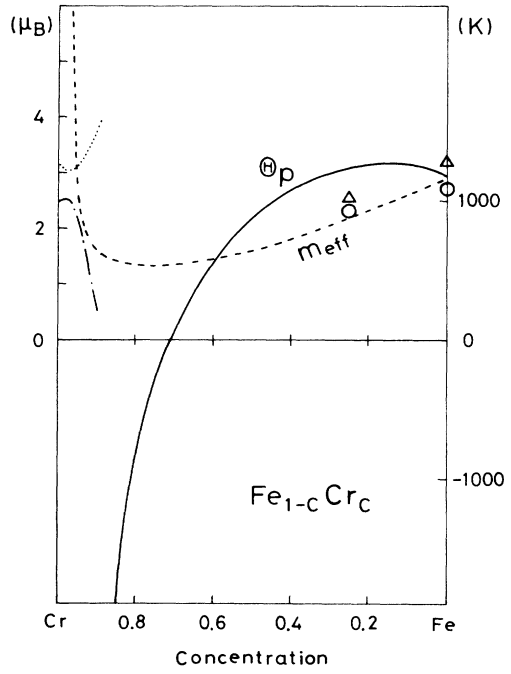

FIG. 14. Effective Bohr magneton number (m_{eff}) and the Weiss constant (Θ_p) evaluated at 1350 K. m_{eff} and the Weiss constant (Θ_N) in the staggered susceptibilities are also shown by dotted and dashed-dotted lines, respectively. Experimental data (Refs. 58 and 59) are shown by open circles (m_{eff}) and triangles (Θ_p), respectively.

creasing Cr concentration, showing a simple dilution picture. When the concentration exceeds 75 at. % Cr the alloys change from the strong to the weak magnetism. Thus m_{eff} being to increase rapidly. This behavior has also been found in Fe-V alloys.[20] Effective Bohr magneton numbers in the staggered susceptibilites also have large values, more than $3\mu_B$ in 90–100 at. % Cr, revealing a characteristic of the weak magnetism. There are only a few experimental data, unfortunately. Therefore it is impossible to make comparison with the experiments at present.

The concentration dependence of partial susceptibilities (χ_α) of constituent atoms is shown in Figs. 15(a) and 15(b). χ_{Fe} follows the Curie-Weiss law in the wide range of concentration. The Cr susceptibilities change their sign except for those at $c=0.9$ and 1.0 with decreasing T, and negatively diverge at T_C. Hasegawa[8] found a positive divergence of χ_{Cr} at T_C in pure Fe. Such a positive divergence is not found in the present calculation.

We show an example of paramagnetic susceptibilities in each environment in Fig. 16. Susceptibilities of Fe LM's follow the Curie-Weiss law. The Fe LM's with fewer Fe NN's have a smaller induced local magnetization. The susceptibilities of Cr LM's in each environment do not follow the Curie-Weiss law. χ_{Cr} with no Fe NN diverge

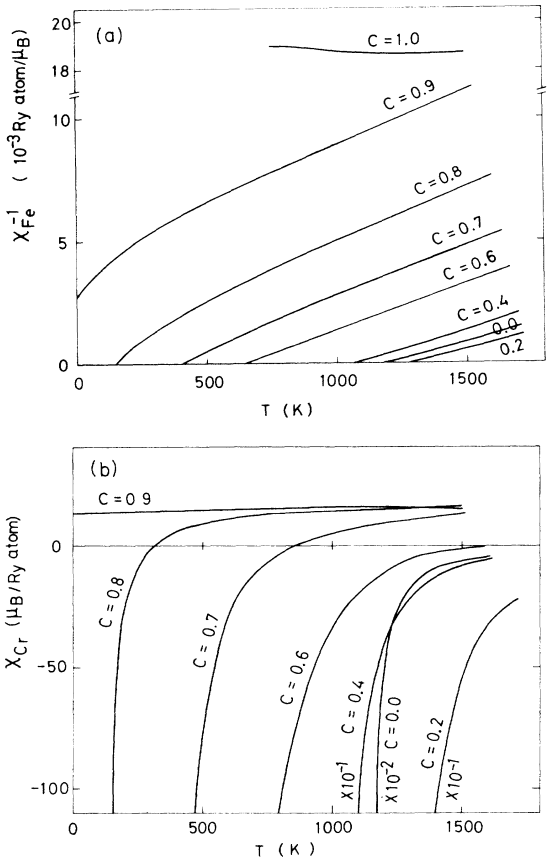

FIG. 15. Paramagnetic spin susceptibilities for (a) Fe and (b) Cr. Note that χ_{Cr} for $C=0.0$, 0.2, and 0.4 are multiplied by 0.01, 0.1, and 0.1, respectively, in the figure.

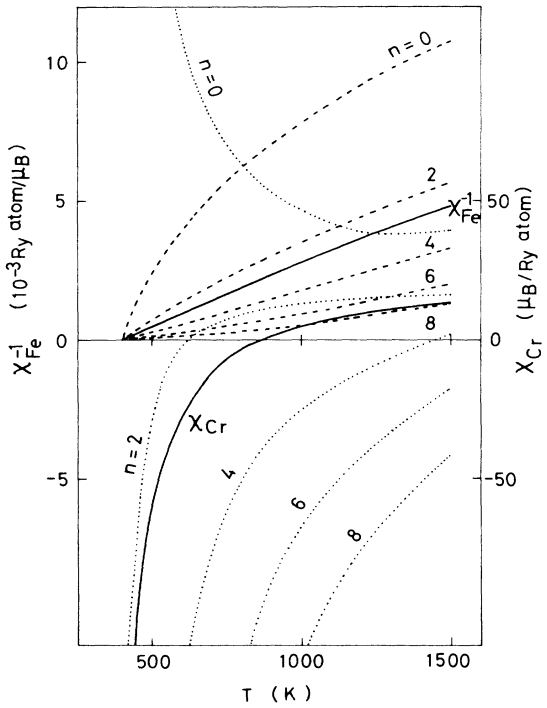

FIG. 16. Temperature variation of the inverse susceptibilities of Fe (dashed curves) and susceptibilities of Cr (dotted curves) for various environments at 70 at. % Cr. Partial susceptibilities for Fe and Cr are also shown by the solid curves.

as the alloy approaches the Curie temperature, while other susceptibilities of Cr change their sign and show a negative divergence at T_C. This is explained as follows. Fe LM show the LM feature rather than the weak magnetic one in this concentration. When the alloy approaches T_C the local magnetizations of Fe induced by the magnetic field become very large as compared with those of Cr LM, because the directional spin fluctuations take place in Fe LM. Then a negative polarization is induced in Cr atom by the surrounding Fe LM via the antiferromagnetic coupling $\mathcal{J}_{\text{FeCr}}$ (<0). Thus Cr LM's show a negative divergence at T_C. For the Cr LM's with no Fe NN's there is no such mechanism. Thus one expects a normal behavior for it.

VIII. SUMMARY AND DISCUSSION

We have extended the theory of LEE at finite temperatures to the antiferromagnetic case and investigated the finite-temperature antiferromagnetism as well as the ferromagnetism in Fe-Cr alloys.

The theory explains qualitatively the magnetic properties of Fe-Cr alloys. A small maximum at 5 at. % Cr in T_C was explained by the enhancement of Fe-Fe exchange coupling due to the alloying effect. With increasing Cr concentration the alloys monotonically approach to the weak magnetic regime. The Curie temperature and magnetization decrease monotonically in 10–80 at. % Cr. The effective Bohr magneton numbers follow a simple di-

lution picture. However each Fe LM is strongly influenced by the surrounding atomic configuration because of the existence of the holes in the up spin DOS. The distribution of Fe LM's is extended from $0\mu_B$ to $2\mu_B$ in the concentrated alloys (60–75 at. % Cr). It causes a broad internal field distribution seen by Fe in agreement with experiments. But further theoretical investigations are desired to discuss the details of the line shape at low temperatures. It has also been verified that the LM with different environments respond to the magnetic field in different ways. In particularly, the Cr LM with no Fe NN's show a positive divergence at T_C, while the Cr with Fe NN's diverge to minus infinity.

In the antiferromagnetic state the alloys show a gap near the Fermi level in the DOS. Such a nesting effect produces a deep minimum of the single-site energy functional $E_{\mathrm{Fe}}(\xi)$, resulting in Fe LM's parallel to the sublattice magnetization even if they are surrounded by eight Fe LM's. With increasing Fe concentration a gap disappears at about 5 at. % Fe, and the minimum in the single-site energy functional $E_{\mathrm{Fe}}(\xi)$ becomes shallow. Then the ferromagnetic Fe-Fe exchange interactions begin to break the antiferromagnetic long-range order. Fe LM show a strong LEE there, i.e., the coexistence of ferromagnetic and antiferromagnetic Fe clusters.

In a small concentration regime between the ferromagnetic and antiferromagnetic states, most of Cr atoms lose the LM at low temperatures but Fe atoms still have them. We only took account of the nearest-neighbor-pair interactions to describe the fluctuations of LM due to the atomic configurations, and moreover $\mathcal{J}_{\mathrm{CrCr}}=\mathcal{J}_{\mathrm{CrFe}}=0$ and $\mathcal{J}_{\mathrm{FeFe}}>0$ at $T=0$. Thus the present calculations do not produce the spin-glass state observed at low temperatures (~ 10 K) in a small concentration regime 81–84 at. % Cr. It is plausible for the following reasons that the long-range Fe-Fe pair interactions produce such a spin-glass state. Chromium is not far away from iron in the Periodic Table. Therefore we do not expect the dumping of long-range interactions due to disorder scattering. Since the Cr LM's disappear at low temperatures and Fe LM's are rather weak in the spin-glass concentration range, we do not expect dumping of the exchange interactions due to disordered LM's either. Thus we might expect to have extended exchange interactions between Fe LM's at low temperatures in the Cr-rich Fe-Cr alloys. It is highly desirable to check by means of the CPA–Korringa-Kohn-Rostoker method[60] whether or not the second-NN exchange interaction between Fe LM's is antiferromagnetic in the spin-glass concentration range.

Finally, we remark that the present theory does not describe a sharp peak of the linear-in-T specific heat at low temperatures near the critical concentration for ferromagnetism.[61] Two mechanisms have been proposed from quite different viewpoints. One is paramagnon mass enhancement in a nearly ferromagnetic metal.[62] The other arises from the existence of localized moments in an infinitely small effective field which results from the long-range exchange interactions and the randomness of the alloy.[63] It is certainly an interesting question in the localized-versus-itinerant magnetism of transition metals which mechanism determines the anomalous Sommerfeld term of the Fe-Cr alloy. One has to go beyond the present framework of the theory, i.e., the static approximation in order to answer this question.

APPENDIX: DERIVATION OF THE ENERGY FUNCTIONAL (2.9)

We explain in this Appendix how Eq. (2.9) follows from Eq. (2.3). We introduce the charge potentials $\{w_i(\xi)\}$ defined by

$$w_i(\xi)\equiv\tfrac{1}{2}\tilde{U}_i(\zeta_i(\xi)-\zeta_i^0) \ . \tag{A1}$$

Here a constant ζ_i^0 will be defined later. We rewrite the energy functional (2.3) using the new potential (A1). Then we obtain

$$E(\xi)=-\beta^{-1}\ln \mathrm{Tr}(e^{-\beta H(\xi)}) + \sum_i \left[-w_i(\xi)\zeta_i^0-\frac{1}{\tilde{U}_i}w_i(\xi)^2+\tfrac{1}{4}\tilde{J}_i\xi_i^2 \right] . \tag{A2}$$

Here we have omitted the constant term $(\sum_i \tilde{U}_i(\zeta_i^0)^2)/4$. $H(\xi)$ in Eq. (A2) is defined by Eq. (2.5) in which $\epsilon_i^0+\tilde{U}_i\zeta_i^0/2-\mu$ has been replaced by $\epsilon_i^0-\mu$.

The saddle-point condition $\partial E/\partial\zeta_i=0$ reduces to $\partial E/\partial w_i=0$. This leads to the following equations:

$$\zeta_i^0=n_i^0(\epsilon_i^0-\mu+w_i)-\frac{2}{\tilde{U}_i}w_i \ . \tag{A3}$$

Here $n_i^0(\epsilon_i^0-\mu+w_i)$ denotes the thermal average of the electron number on site i with respect to the one-electron Hamiltonian $H(\xi)$.

We now define ζ_i^0 so that $\{w_i(\xi)\}$ vanish at $T=0$:

$$\zeta_i^0=[n_i^0(\epsilon_i^0-\mu)]_{T=0} \ . \tag{A4}$$

This is nothing else but the electron number on site i in the Hartree-Fock approximation at $T=0$. In the strong $\tilde{U}_i$ limit the charge neutrality condition $\zeta_i^0=n_i$ may be satisfied on each site. Then Eq. (A3) reduces to

$$n_i^0(\epsilon_i^0-\mu+w_i)=n_i \ , \tag{A5}$$

and Eq. (A2) reduces to

$$E(\xi)=-\beta^{-1}\ln \mathrm{Tr}(e^{-\beta H(\xi)})+\sum_i(-w_in_i+\tfrac{1}{4}\tilde{J}_i\xi_i^2) \ . \tag{A6}$$

Equation (A5) determines the charge potential $w_i(\xi)$ for a given set of exchange fields $\{\xi_i\}$.

The free energy for the one-electron Hamiltonian in Eq. (A6) is expressed as follows:

$$-\beta^{-1}\ln \mathrm{Tr}(e^{-\beta H(\xi)})=-\beta^{-1}\int d\omega\,\rho(\omega,\xi)\ln(1+e^{-\beta\omega}) \ . \tag{A7}$$

Here $\rho(\omega,\xi)$ is the density of states for $H(\xi)$. By making use of integration, by parts, we obtain

$$-\beta^{-1}\ln \mathrm{Tr}(e^{-\beta H(\xi)})=-\int d\omega\, f(\omega)\int_{-\infty}^{\omega}\rho(\omega',\xi)d\omega' \ , \tag{A8}$$

where $f(\omega)$ is the Fermi distribution function.

The integrated number of states is written as follows:

$$\int_{-\infty}^{\omega}\rho(\omega',\xi)d\omega'=\int_{-\infty}^{\omega}\frac{(-)}{\pi}\mathrm{Im}\sum_{k\sigma}\frac{1}{\omega'+i\delta-\epsilon_{k\sigma}}d\omega'$$

$$=-\frac{1}{\pi}\mathrm{Im\,Tr\ln}[z-\mathbf{H}(\xi)]\ , \qquad \text{(A9)}$$

$$[\mathbf{H}(\xi)]_{i\nu j\nu'\sigma}\equiv[\epsilon_i^0-\mu+w_i(\xi)-\tfrac{1}{2}\tilde{J}_i\xi_i\sigma-h_i\sigma]$$

$$\times\delta_{ij}\delta_{\nu\nu'}+t_{i\nu j\nu'}\ . \qquad \text{(A10)}$$

Here $\epsilon_{k\sigma}$ denotes a one-electron energy level for the Hamiltonian $H(\xi)$. The complex number z is defined by $\omega+i\delta$, δ being an infinitesimal positive number.

Note that

$$z-\mathbf{H}(\xi)=r^*(L^{-1})r-r^*t^0r \qquad \text{(A11)}$$

when we assume a geometrical average for the transfer integral. Here $(r^*)_{i\nu j\nu'}=r_{i\nu}^*\delta_{ij}\delta_{\nu\nu'}$ and $(r)_{i\nu j\nu'}=r_{i\nu}\delta_{ij}\delta_{\nu\nu'}$, $r_{i\nu}$ being an off-diagonal factor.[37] The matrix $(t^0)_{i\nu j\nu'}$ denotes a transfer integral for a pure metal. The locator matrix L is defined by Eq. (2.10). Then Eq. (A9) reduces to

$$\int_{-\infty}^{\omega}\rho(\omega',\xi)d\omega'$$

$$=-\frac{1}{\pi}\mathrm{Im}[\mathrm{Tr\ln}(L^{-1}-t^0)+\mathrm{Tr\ln}(r^*r)]\ . \qquad \text{(A12)}$$

The second term at the right-hand side of Eq. (A12) vanishes because it is real. Thus Eq. (A8) is expressed finally as

$$-\beta^{-1}\ln\mathrm{Tr}(e^{-\beta H(\xi)})=\frac{1}{\pi}\int d\omega f(\omega)\mathrm{Im\,Tr\ln}(L^{-1}-t^0)\ . \qquad \text{(A13)}$$

Substituting Eq. (A13) into Eq. (A6) we obtain Eq. (2.9).

[1]J. F. Janak, Phys. Rev. B **16**, 255 (1977).
[2]J. E. Goldman and R. Smoluchowski, Phys. Rev. **75**, 140 (1947).
[3]V. Jaccarino and L. R. Walken, Phys. Rev. Lett. **15**, 258 (1965).
[4]J. S. Kouvel, in *Magnetism and Metallurgy*, edited by A. E. Berkowitz and E. Kneller (Academic, New York, 1969), Vol. 2.
[5]H. Miwa, J. Magn. Magn. Mater. **10**, 223 (1979).
[6]J. W. Cable and H. R. Child, Phys. Rev. B **10**, 4607 (1974).
[7]S. F. Edwards and P. W. Anderson, J. Phys. F **5**, 965 (1975).
[8]H. Hasegawa, J. Phys. Soc. Jpn. **50**, 802 (1981).
[9]Y. Kakehashi, J. Phys. Soc. Jpn. **50**, 3177 (1981); **51**, 94 (1982).
[10]Y. Kakehashi, J. Magn. Magn. Mater. **37**, 189 (1983).
[11]R. L. Stratonovich, Docl. Akad. Nauk. SSSR **115**, 1097 (1958) [Sov. Phys.—Dokl. **2**, 416 (1958)].
[12]J. Hubbard, Phys. Rev. Lett. **3**, 77 (1959).
[13]M. Cyrot, Phys. Rev. Lett. **25**, 871 (1970); J. Phys. (Paris) **33**, 125 (1972).
[14]J. Hubbard, Phys. Rev. B **19**, 2626 (1979); **20**, 4584 (1979); **23**, 5970 (1981).
[15]H. Hasegawa, J. Phys. Soc. Jpn. **46**, 1504 (1979); **49**, 178 (1980).
[16]F. Matsubara, Prog. Theor. Phys. **52**, 1124 (1974).
[17]S. Katsura, S. Fujiki, and S. Inawashiro, J. Phys. C **12**, 2839 (1979).
[18]Y. Kakehashi, J. Phys. Soc. Jpn. **52**, 637 (1983).
[19]Y. Kakehashi, J. Magn. Magn. Mater. **43**, 79 (1984).
[20]Y. Kakehashi, Phys. Rev. B **32**, 3035 (1985).
[21]S. K. Burke, R. Cywinski, J. R. Davis, and B. D. Rainford, J. Phys. F **13**, 451 (1983).
[22]C. Fincher, S. M. Shapiro, A. H. Palumbo, and R. D. Parks, Phys. Rev. Lett. **45**, 474 (1980).
[23]M. Hansen, *Constitution of Binary Alloys* (McGraw-Hill, New York, 1958).
[24]I. R. Herbert, P. E. Clark, and G. V. H. Wilson, J. Phys. Chem. Solids **33**, 979 (1972).
[25]M. Shiga and Y. Nakamura, J. Phys. Soc. Jpn. **49**, 528 (1980).
[26]S. M. Dübiel, Ch. Sauer, and W. Zinn, Phys. Rev. B **30**, 6285 (1984).
[27]S. M. Dübiel, Ch. Saver, and W. Zinn, Phys. Rev. B **32**, 2745 (1985).
[28]M. Mori, Y. Tsunoda, and N. Kunitomi, Solid State Commun. **18**, 1103 (1976).
[29]S. K. Burke and B. D. Rainford, J. Phys. F **8**, L239 (1978).
[30]T. Cey and N. Kunitomi, J. Phys. Soc. Jpn. **51**, 3073 (1982).
[31]H. Hasegawa and J. Kanamori, J. Phys. Soc. Jpn. **33**, 1607 (1972).
[32]G. Frollani, F. Menzinger, and F. Sacchetti, Phys. Rev. B **11**, 2030 (1975).
[33]T. Jo, J. Phys. Soc. Jpn. **51**, 794 (1982).
[34]Y. Kakehashi, Phys. Rev. B **34**, 3243 (1986).
[35]Y. Kakehashi and P. Fulde, Phys. Rev. B **32**, 1595 (1985).
[36]S. Q. Wang, W. E. Evenson, and J. R. Schrieffer, Phys. Rev. Lett. **23**, 92 (1969); J. Appl. Phys. **41**, 1199 (1970).
[37]H. Shiba, Prog. Theor. Phys. **46**, 77 (1971).
[38]Y. Kakehashi, J. Phys. Soc. Jpn. **50**, 1505 (1981).
[39]J. M. Cowley, Phys. Rev. **77**, 669 (1950).
[40]A. Z. Menshikov and E. E. Yarchikov, Zh. Eksp. Theor. Fiz. **63**, 190 (1972) [Sov. Phys.—JETP **36**, 100 (1973)].
[41]E.-N. Foo and H. Amar, Phys. Rev. Lett. **25**, 1748 (1970).
[42]M. Plischke and D. Mattice, Phys. Rev. B **7**, 2430 (1973).
[43]D. G. Pettifor, Comput. Coupling Phase Diagrams & Thermochem. (GB) **1**, 305 (1977).
[44]J. Kübler, J. Magn. Magn. Mater. **20**, 277 (1980).
[45]A. Arrott, S. A. Werner, and H. Kendrick, Phys. Rev. **153**, 624 (1967).
[46]Y. Ishikawa, S. Hoshino, and Y. Endoh, J. Phys. Soc. Jpn. **22**, 1221 (1967).
[47]Y. Kakehashi, J. Phys. Soc. Jpn. **50**, 2251 (1981); **50**, 3620 (1981).
[48]K. Usami and T. Moriya, J. Magn. Magn. Mater. **20**, 171 (1980).
[49]S. A. Werner, A. Arrott, and H. Kendrick, Phys. Rev. Lett. **14**, 1022 (1965); Phys. Rev. **155**, 528 (1967).
[50]A. Bieber and F. Gautier, Solid State Commun. **39**, 149 (1981); J. Phys. Soc. Jpn. **53**, 2061 (1984).
[51]T. Oguchi, K. Terakura, and N. Hamada, J. Phys. F **13**, 145 (1983).

[52]A. T. Aldred, Phys. Rev. B **14**, 219 (1976).
[53]A. T. Aldred, B. D. Rainford, J. S. Kouvel, and T. J. Hicks, Phys. Rev. B **14**, 228 (1976).
[54]G. H. Lander and L. Heaton, J. Phys. Chem. Solids **32**, 427 (1971).
[55]Previous results for the amplitudes of LM's in Refs. 9, 10, and 18–20 should be corrected by using Eq. (2.44).
[56]M. Yasui and M. Shimizu, J. Phys. F **9**, L227 (1979).
[57]J. Friedel and L. E. Hedmann, J. Phys. (Paris) **39**, 1225 (1978).
[58]M. Fallot, J. Phys. Radium **5**, 153 (1944).
[59]Y. Nakagawa, J. Phys. Soc. Jpn. **11**, 855 (1956).
[60]G. M. Stocks, W. M. Temmermann, and B. L. Gyorffy, Phys. Rev. Lett. **41**, 339 (1978).
[61]C. T. Wei, C. H. Cheng, and P. A. Beck, Phys. Rev. Lett. **2**, 95 (1959).
[62]E. Bucher, W. F. Brinkman, J. P. Maita, and H. J. Williams, Phys. Rev. Lett. **18**, 1125 (1967).
[63]W. Marshall, Phys. Rev. B **118**, 1519 (1960).